

draft of November 13, 2018

# Propagation of Ultra-High-Energy Protons through the Magnetized Cosmic Web

Santabrata Das<sup>1</sup>, Hyesung Kang<sup>2,3</sup>, Dongsu Ryu<sup>4</sup>, and Jungyeon Cho<sup>4</sup>

## ABSTRACT

If ultra-high-energy cosmic rays (UHECRs) originate from extragalactic sources, understanding the propagation of charged particles through the magnetized large scale structure (LSS) of the universe is crucial in the search for the astrophysical accelerators. Based on a novel model of the turbulence dynamo, we estimate the intergalactic magnetic fields (IGMFs) in cosmological simulations of the formation of the LSS. Under the premise that the sources of UHECRs are strongly associated with the LSS, we consider a model in which protons with  $E \geq 10^{19}$  eV are injected by sources that represent active galactic nuclei located inside clusters of galaxies. With the model IGMFs, we then follow the trajectories of the protons, while taking into account the energy losses due to interactions with the cosmic background radiation. For observers located inside groups of galaxies like ours, about 70% and 35% of UHECR events above 60 EeV arrive within  $\sim 15^\circ$  and  $\sim 5^\circ$ , respectively, of the source position with time delays of less than  $\sim 10^7$  yr. This implies that the arrival direction of super-GZK protons might exhibit a correlation with the distribution of cosmological sources on the sky. In this model, nearby sources (within 10 – 20 Mpc) should contribute significantly to the particle flux above  $\sim 10^{20}$  eV.

*Subject headings:* cosmic rays – large scale structure of the universe – magnetic fields – methods: numerical

---

<sup>1</sup>Astrophysical Research Center for the Structure and Evolution of the Cosmos, Sejong University, Seoul 143-747, South Korea: sbdas@canopus.cnu.ac.kr

<sup>2</sup>Department of Earth Sciences, Pusan National University, Pusan 609-735, South Korea: kang@uju.es.pusan.ac.kr

<sup>3</sup>Author to whom correspondence should be addressed

<sup>4</sup>Department of Astronomy and Space Science, Chungnam National University, Daejeon 305-764, South Korea: ryu@canopus.cnu.ac.kr, cho@canopus.cnu.ac.kr

## 1. Introduction

Over the past several decades, significant progress has been made on both theoretical and observational fronts in understanding the nature and origin of ultrahigh energy cosmic rays (UHECRs), those with  $E \gtrsim 1$  EeV ( $= 10^{18}$  eV) (for recent reviews, see Nagano & Watson 2000; Berezhinsky *et al.* 2006). Yet, the acceleration mechanism and the corresponding astrophysical “accelerators” of these energetic particles are still largely unknown. Observational data from several experiments such as the High Resolution Fly’s Eye (HiRes) indicate that the mass composition of UHECRs becomes lighter at higher energies (Abbasi *et al.* 2005). However, composition analyses that include high energy interactions are often model-dependent and inconclusive (Watson 2006). According to a recent report from the Pierre Auger Observatory, the mass composition is likely mixed, possibly becoming heavier above 30 EeV (Unger *et al.* 2007). The overall distribution of UHECR arrival directions is considered to be consistent with isotropy (Burgett & O’Malley 2003). Exceptions to this general isotropy include the small-scale clusterings of doublets and triplets found in data collected by the Akeno Giant Air Shower Array (AGASA) experiment (Takeda *et al.* 1999; Uchihori *et al.* 2000). In addition, a possible correlation of AGASA events with BL Lacertae objects has been suggested (Tinyakov & Tkachev 2001). But these claims have been confirmed neither by HiRes (Abbasi *et al.* 2006) nor by Auger (Harari *et al.* 2007; Armengaud *et al.* 2007). However, the Auger Collaboration recently reported that the arrival directions of UHECRs above 60EeV in their data show a correlation with the position of active galactic nuclei (AGNs) lying within 75 Mpc (Abraham *et al.* 2007).

Since protons with  $E \gtrsim 1$  EeV cannot be confined within the Galactic plane, UHECRs likely originate from extragalactic sources. In particular, the overall isotropy of arrival directions suggests that there may be a large number of sources distributed over cosmological distances (Nagano & Watson 2000; Burgett & O’Malley 2003). During their propagation through intergalactic space, such protons will lose energy by means of pion and pair production processes while interacting with the cosmic background radiation (Greisen 1966; Zatsepin & Kuzmin 1966). The flux of ultra-high-energy (UHE) protons from cosmological sources is thus expected to be strongly attenuated, resulting in a significant suppression in the observed spectrum above the GZK threshold energy,  $E_{\text{GZK}} \approx 40$  EeV (Berezhinsky *et al.* 2006). Although the AGASA data show no indication of the GZK suppression (Nagano & Watson 2000), both the Yakutsk Extensive Air Shower array and HiRes have reported a suppression of flux above  $E_{\text{GZK}}$ , contradicting the AGASA finding (Pravdin *et al.* 1999; Zech 2004). Indeed the same suppression was seen in a recent Auger measurement (Facal *et al.* 2007), which seems to have ended the controversy over the presence of the GZK cutoff. The so-called dip-calibrated UHECR spectra from different experiments compiled by Berezhinsky *et al.* (2006), appear to be in good agreement with each

other and to be consistent with GZK suppression. However, it has yet to be understood whether this suppression is actually due to the GZK cutoff or due to the maximum acceleration energy,  $E_{\text{max}}$ , of astrophysical accelerators. If UHECRs are protons, the GZK energy loss should operate at acceleration sites as well, leading to an  $E_{\text{max}}$  close to  $E_{\text{GZK}}$  (see, *e.g.*, Kang *et al.* 1997).

Most UHE protons observed above the GZK energy must come from within the so-called GZK sphere of radius  $R_{\text{GZK}} \sim 100$  Mpc, although the proton interaction length at  $E_{\text{GZK}}$  is  $l_{40\text{EeV}} \approx 1$  Gpc, corresponding to  $z \sim 0.2$  (Berezinsky & Grigor’eva 1988). However, finding cosmological sources inside the GZK sphere from the arrival directions of UHECRs is not straightforward, since their paths are deflected by intergalactic magnetic fields (IGMFs) (*e.g.* Sigl *et al.* 2003; Dolag *et al.* 2004). Sigl and collaborators have extensively studied the propagation of UHECRs in a structured and magnetized universe, adopting a numerical model for the IGMFs (Sigl *et al.* 2003, 2004; Armengaud *et al.* 2005). In this model, the IGMFs are generated by means of the Biermann “battery” mechanism at shocks and then evolved passively in a cosmological hydrodynamic simulation (Kulsrud *et al.* 1997; Ryu *et al.* 1998). The strength of the resulting fields is rescaled to match the simulated field strength in Coma-like clusters to the observed strength, which is on the order of microgauss. UHECRs with  $E \geq 10\text{EeV}$  are then injected at cosmological sources. These particles propagate through the magnetized large scale structure (LSS) of the universe, and arrive at a mock observer with deflection angle  $\theta$ , the angle between the arrival direction and the source’s location on the sky. Sigl *et al.* found that the deflection due to IGMFs is significant, with  $\theta \gtrsim 20^\circ$  above 100 EeV. On the other hand, Dolag *et al.* adopted an IGMF model from a “constrained” cosmological simulation employing a magnetohydrodynamic (MHD) version of a smoothed particle hydrodynamics (SPH) code. They found the deflection angle of protons with 100 EeV to be less than  $1^\circ$ , contradicting the estimate by Sigl *et al.* (Dolag *et al.* 2004, 2005).

This controversy over the predicted deflection angles demonstrates the importance of modeling the IGMFs in identifying the astrophysical sources and studying the origin of UHECRs. In order to reexamine this issue, here we adopt IGMFs, based on a novel models of the turbulence dynamo Ryu *et al.* (2008) In this model, the strength of the magnetic fields is estimated from the local vorticity and turbulent kinetic energy in cosmological structure formation simulations. For the field direction, the passive fields from these simulations are used.

The maximum energy of nuclei of charge  $Z$  that can be confined and accelerated by

astrophysical sources is given by

$$E_{\max} \approx Z \left( \frac{V}{c} \right) \left( \frac{B}{\mu\text{G}} \right) \left( \frac{L}{\text{kpc}} \right) 10^3 \text{EeV}, \quad (1)$$

where  $V$ ,  $B$ , and  $L$  are the characteristic flow speed, magnetic field strength, and linear size of the accelerator, respectively (Hillas 1984). There are a few viable candidates that can produce the required  $E_{\max} \sim 100$  EeV: jets from AGNs (*e.g.*, Biermann & Strittmatter 1987), gamma-ray bursts (*e.g.*, Waxman 1995), and cosmological shocks (Kang *et al.* 1996, 1997). In this study, we consider AGNs inside galaxy clusters as the sources of UHECRs. Thus, the source position is in effect correlated with the LSS of the universe. Protons with  $E \geq 10$  EeV are injected at the sources and travel through the simulated magnetized space until they lose energy down to 10 EeV, meanwhile visiting mock observers placed inside groups of galaxies. In this study we focus mainly on the deflection angle, the time delay relative to rectilinear flight, and the energy spectrum of the UHE protons.

In the next section, we describe our model IGMFs, cosmic-ray sources, and observers, and the simulations of the propagation of UHE protons in intergalactic space. The results are presented in §3. Finally, we conclude in §4.

## 2. Models and Methods

### 2.1. Intergalactic Magnetic Fields

Our cosmological hydrodynamic simulations of a concordance  $\Lambda$ CDM universe are carried out with the following parameters:  $\Omega_{\text{BM}} = 0.043$ ,  $\Omega_{\text{DM}} = 0.227$ , and  $\Omega_{\Lambda} = 0.73$ ,  $h \equiv H_0/(100 \text{ km/s/Mpc}) = 0.7$ , and  $\sigma_8 = 0.8$ . A cubic box of comoving size  $100 h^{-1}\text{Mpc}$  is simulated using  $512^3$  grid zones for gas and gravity and  $256^3$  particles for dark matter. In the simulation, magnetic fields are generated through the Biermann battery mechanism at structure formation shocks and then evolved passively with the flow motions (Kulsrud *et al.* 1997; Ryu *et al.* 1998). The simulation was repeated for six different realizations of the initial conditions to examine the effects of cosmic variance. Non gravitational effects, including radiative cooling, photo ionization and heating, and feedback from star formation are ignored. Those processes affect the generation and evolution of magnetic fields mainly on small scales (Kang *et al.* 2007), which should not alter the large-scale fields primarily responsible for the deflection of UHECRs.

In principle, if we were to perform full MHD simulations, we could follow the growth of the IGMFs through stretching, twisting, and folding of field lines, the process known as the turbulence dynamo. In practice, however, the computational resources currently

available do not allow high enough numerical resolution to reproduce the full development of MHD turbulence: since the numerical resistivity is larger than the physical resistivity by many orders of magnitude, the growth of the magnetic fields saturates before the dynamo action becomes fully operative (Kulsrud *et al.* 1997). So, Sigl *et al.* (2003, 2004) rescaled the strength of their passively evolved fields in the postprocessing analysis to match the observed field strength in clusters of galaxies. This rescaling, which hinges on the observed field strength in the intracluster medium, does not necessarily result in correct field strengths for filaments, sheets, and voids. On the other hand, in the MHD SPH simulations of Dolag *et al.* (2004, 2005), the initial field strength was adjusted to obtain a microgauss level in clusters of galaxies at the present epoch. They demonstrated that their simulated cluster fields are consistent with various observations, such as rotation measure profiles and the total radio powers of cluster halos. A lack of observations, however, prevents their simulated fields in low-density regions from being tested against the real magnetic fields in filaments and sheets. In the MHD SPH simulations, the flow motions can be resolved reasonably well in high-density regions, where the smoothing length is sufficiently small, ensuring adequate growth of magnetic fields. However, turbulence may not be fully realized in the low-density regions, which have large smoothing lengths, so the field strength in filaments and sheets may be underestimated in such simulations.

In this study, we take a new approach detailed in Ryu *et al.* (2008). If one assumes that magnetic fields grow as a result of the turbulence dynamo, their energy density can be estimated from the eddy turnover number and turbulent energy density as follows :

$$\varepsilon_B = \phi \left( \frac{t}{t_{\text{eddy}}} \right) \varepsilon_{\text{turb}}. \quad (2)$$

Here the eddy turnover time is defined as the reciprocal of the vorticity at driving scales,  $t_{\text{eddy}} \equiv 1/\omega_{\text{driv}}$  ( $\vec{\omega} \equiv \vec{\nabla} \times \vec{v}$ ), and  $\phi$  is the conversion factor from turbulent to magnetic energy, which is determined from high-resolution MHD simulations of turbulence. For our model IGMFs, the number of eddy turnovers is estimated as the age of the universe multiplied by the magnitude of the local vorticity, that is,  $t_{\text{age}}\omega$ . The local vorticity and turbulent energy density are calculated from the cosmological structure formation simulations. The energy density given by equation (2) fixes the strength of the IGMFs, so our model requires neither rescaling of the field strength nor adjustment of the initial fields. As in the work of Sigl *et al.*, we assume that the topology of the IGMFs in the LSS can be represented statistically by the topology of the passive magnetic fields in the cosmological simulations.

Figure 1 shows a two-dimensional slice of the magnetic field strength in our model at the present epoch. The IGMFs are structured and well correlated with the weblike cosmic distribution of matter. The strongest magnetic fields, with  $B \gtrsim 0.1\mu\text{G}$ , are found inside and

around clusters, while the fields are weaker in filaments, sheets, and voids. Overall, there is a correlation between field strength and gas density, as can be seen in Figure 2(*left*). In the regions of galaxy clusters, with  $\rho_{\text{gas}}/\langle\rho_{\text{gas}}\rangle \gtrsim 10^3$ , we find  $\langle B \rangle \sim 1 \mu\text{G}$ . For typical filamentary regions, with  $\rho_{\text{gas}}/\langle\rho_{\text{gas}}\rangle \sim 10$ , the field has  $\langle B \rangle \sim 10^{-8} \text{ G}$ . By comparison, the average field strength in filaments is found to be  $\langle B \rangle \sim 10^{-7} \text{ G}$  by Sigl *et al.* (2004) and  $\langle B \rangle \sim 10^{-10} \text{ G}$  by Dolag *et al.* (2005). The right panel of Figure 2 shows the volume fraction,  $df/d\log B$  (*solid line*), and its cumulative distribution,  $f(> B)$  (*dotted line*) and  $f(< B)$  (*dot-dashed line*). In our model, the volume filling factor for  $B > 10^{-8} \text{ G}$  is  $f(> 10^{-8} \text{ G}) \approx 0.01$ . By comparison,  $f(> 10^{-8} \text{ G}) \approx 0.1$  in Sigl *et al.* (2004) and  $f(> 10^{-8} \text{ G}) \approx 10^{-4}$  in Dolag *et al.* (2005). Hence, the field strength in filaments in our model lies in the middle of the values from the models used by these two groups, that is, lower than Sigl *et al.*'s but higher than that of Dolag *et al.*'s.

## 2.2. AGNs as UHECR Sources

In the framework of bottom-up acceleration models, AGNs are the most studied candidate astrophysical accelerators to produce cosmic-ray nuclei beyond the GZK energy (for a review, see Berezhinsky *et al.* 2006). As noted in §I, it has also been suggested that cosmological shocks may accelerate nuclei of charge  $Z$  up to an  $E_{\text{max}}$  of a few times  $10^{19} Z \text{ eV}$ , but it is unlikely that protons would be accelerated beyond the GZK energy by such shocks (Kang *et al.* 1997; Inoue *et al.* 2007). However, if some UHECRs are iron nuclei, cosmological shocks can provide the acceleration sites for super-GZK cosmic rays (Inoue *et al.* 2007). In this paper, we consider only AGN-like objects as sources of UHECRs, since we focus on the propagation of UHE protons.

We identify X-ray clusters characterized by the X-ray emission weighted gas temperature  $kT > 1 \text{ keV}$  in the cosmological simulations as source locations. One AGN is placed at the center of each “host” cluster. With this selection criterion, the source locations are chosen, in effect, at high-density regions with the strongest field strength. Table 1 shows the number of such clusters found in the six cosmological simulations ( $\Lambda\text{CDM1}$ - $\Lambda\text{CDM6}$ ) with different initial conditions. The three-dimensional distribution of the 18 sources in  $\Lambda\text{CDM1}$  is shown in Figure 3. Given the simulation volume of  $(100 h^{-1}\text{Mpc})^3$ , the mean separation of sources is  $l_s \approx 40 h^{-1}\text{Mpc}$  and the source number density is  $n_s = 2 - 3 \times 10^{-5} h^3\text{Mpc}^{-3}$ , which is consistent with the required UHECR source density inferred from the small-scale clustering found in the AGASA data (Yoshiguchi *et al.* 2003; Sigl *et al.* 2003; Blasi & De Marco 2004). The field strength at the source locations mostly lies in the range  $0.1\mu\text{G} \lesssim B_s \lesssim 2\mu\text{G}$ , with a peak at  $\sim 1\mu\text{G}$ ; its distribution is shown in Figure 4 (*left*).

### 2.3. Groups of Galaxies as Mock Observers

The key physical condition for an “observer” that is most relevant to this study is the strength and direction of the magnetic fields, since we are interested primarily in the deflection angles and time delays of UHECRs. Little is known about the magnetic fields in the intergalactic space within the Local Group. So, we select groups of galaxies identified in the simulation data that have similar halo gas temperatures to the Local Group, that is,  $0.05\text{keV} < kT < 0.5\text{keV}$  (Rasmussen & Pedersen 2001), assuming that these groups are located in magnetic environment similar to that of the Local Group. There are about 1000 – 1400 identified groups with gas temperatures in this range inside the simulation volume (see Table 1). As can be seen in Figure 3, these groups are not distributed uniformly but are located mostly along filaments, following the matter distribution of the LSS. A mock observer, modeled as a sphere of radius  $R_{\text{obs}} = 0.5 h^{-1}\text{Mpc}$ , is placed at each group. The value of  $R_{\text{obs}}$  is chosen so that the observer’s sphere is well contained within the associated filament, since the typical thickness of the magnetized region around a filament is about  $2 - 3 h^{-1}\text{Mpc}$ . If we were to use an  $R_{\text{obs}}$  smaller than the value adopted, smaller cross sections would lead to smaller detection rates of cosmic rays in our numerical experiment described below. The right panel of Figure 4 shows the field strength within the observer spheres for the six cosmological simulations:  $10^{-4}\mu\text{G} \lesssim B_{\text{obs}} \lesssim 0.1\mu\text{G}$  with a peak at  $\sim 10^{-9}$  G. This illustrates the distribution of magnetic field strength in filaments.

### 2.4. Propagation of UHE protons in the Intergalactic Space

The characteristics of the particle spectrum accelerated at UHECR sources are largely unknown. We thus make the simple assumption that the accelerated protons have a power-law energy spectrum at their source:  $N_{\text{inj}}(E_{\text{inj}}) \propto E_{\text{inj}}^{-\gamma}$  for  $10 \text{ EeV} \leq E_{\text{inj}} \leq 10^3 \text{ EeV}$ . In practice,  $\gamma = 0$  is used to generate a flat injection spectrum at the sources, and later a weighting factor proportional to  $E_{\text{inj}}^{-\gamma}$  is applied to the statistics (except for the distribution in Fig. 5; see §3.1 for details). For each  $\Lambda\text{CDM}$  simulation, a total of  $3 \times 10^4$  particles are randomly distributed over the sources and then launched in random directions from random positions inside a sphere of radius  $0.5 h^{-1}\text{Mpc}$ .

We follow the trajectories of the UHE protons by numerically integrating the equations of motion in our model IGMFs,

$$\frac{d\vec{r}}{dt} = \vec{v} ; \quad \frac{d\vec{v}}{dt} = \frac{Ze}{mc} (\vec{v} \times \vec{B}) . \quad (3)$$

The energy losses due to photo pion production and pair production are treated with the

continuous loss approximation (Berezinsky *et al.* 2006), but the adiabatic losses due to cosmic expansion are ignored, because the largest source-to-observer distance is  $D_{\max} \sim 1$  Gpc in our experiment, corresponding to only  $z_{\max} \approx 0.2$ . In practice, the distances are not known in advance, since we are integrating the trajectory from sources to observers.

The simulation box of  $(100 h^{-1} \text{Mpc})^3$  at  $z = 0$  is used to define sources (host clusters), mock observers (groups), and the IGMF data. Additional virtual boxes with the same distribution of mock observers and IGMF data are periodically stacked indefinitely. Particles are injected from the sources only in the original box. Then they travel through the magnetized space consisting of the original box and the replicated periodic boxes. Once a particle visits an observer sphere, the arrival direction, time delay and energy of the particle are registered as a “recorded event.” We let the particle continue its journey, visiting several observers during its full flight, until its energy falls to 10 EeV. With  $3 \times 10^4$  protons injected for each simulation box, about  $2.6 \times 10^5$  events are recorded in total for all six  $\Lambda$ CDM simulations.

In our propagation experiment, the source-to-observer distance  $D$  can be arbitrarily small because the specific way that we set up source and observer locations, and the statistics of recorded events depend on the minimum value of  $D$ . In reality, the closest AGNs to us are Centaurus A, at 3.42 Mpc (Ferrarese *et al.* 2007), in the southern hemisphere and M87, at 16.7 Mpc (Mei *et al.* 2007), in the northern hemisphere. So we mostly present the results for  $D_{\min} = 3$  Mpc or  $D_{\min} = 10$  Mpc. The recorded events with  $D < D_{\min}$  are excluded from the analysis. For  $D_{\min} \geq 10$  Mpc, however, the results become less sensitive to the value of  $D_{\min}$ .

### 3. Results

#### 3.1. Deflection Angle and Time Delay of UHECRs

With a gyroradius

$$r_g = 10 \text{ kpc} \left( \frac{E}{10^{19} \text{eV}} \right) \left( \frac{B}{\mu\text{G}} \right)^{-1}, \quad (4)$$

UHE protons will suffer significant deflection during their propagation when they pass regions with  $B \gtrsim 10^{-8}$  G, that is, clusters and filaments. Here the filamentary regions are more significant players than clusters, since the volume filling factor of filaments is much larger than that of clusters (see Fig. 2). As a result of this deflection, the actual path traveled by the UHECRs in the presence of the IGMFs can be much longer than a rectilinear path, causing a significant time delay. We therefore measure the deflection angle as the angle between the arrival direction of the cosmic rays and the source position on the sky, and the



time delay as the difference between the arrival time and the rectilinear travel time.

UHE protons can be also deflected inside the host clusters of sources, before they escape to intergalactic space. Typical clusters have a magnetized core envelope structure with  $B_{\text{core}} \sim 1\mu\text{G}$ ,  $R_{\text{core}} \lesssim 0.5 h^{-1}\text{Mpc}$  and  $B_{\text{env}} \sim 0.01 - 0.1\mu\text{G}$ , extending out to  $R_{\text{env}} \sim 3 h^{-1}\text{Mpc}$  (see Fig. 1). So, the protons with  $E \lesssim E_{\text{GZK}}$  injected by AGNs are scattered by turbulent magnetic fields inside the host clusters and confined within the magnetized structure for a while. The scatterings by the turbulent fields local to the sources alone can cause a deflection angle

$$\theta_{\text{source}} \sim \tan^{-1} \left( \frac{\text{a few Mpc}}{D} \right), \quad (5)$$

for protons with  $E \lesssim E_{\text{GZK}}$ .

Figure 5 shows the distributions of the deflection angle  $\theta$  and the time delay  $t_d$  as functions of the distance  $D$  for the  $\Lambda\text{CDM1}$  simulation. The events are divided into three channels in observed energy, as follows:  $10 < E_{\text{obs}} < 30$  (*top*),  $30 < E_{\text{obs}} < 60$  (*middle*), and  $E_{\text{obs}} > 60$  (*bottom*), where the particle energy is given in units of EeV. The data points are color-coded by the injection energy in the same three channels, that is, red for  $10 < E_{\text{inj}} < 30$ , blue for  $30 < E_{\text{inj}} < 60$ , and green for  $E_{\text{inj}} > 60$ . For these plots, the calculation was performed with an injection spectrum with  $\gamma = 2.7$  instead of the flat spectrum, since the recorded data points in this type of representation cannot be weighted with a factor proportional to  $E_{\text{inj}}^{-\gamma}$ .

Sub-GZK protons, with  $E_{\text{obs}} < 60$  EeV, come from sources as distant as  $D \sim 1$  Gpc. For these particles, the distribution of  $\theta$  shows a pattern roughly in accord with the diffusive transport limit, but it also indicates a bimodality divided at  $D \sim 15$  Mpc (Fig. 5, *top and middle left*). The events with  $D \lesssim 15$  Mpc are likely to be cases in which both the source and observer belong to the same filament. These particles are more likely to travel through strongly magnetized filaments rather than void regions, resulting in large deflection angles in addition to a large  $\theta_{\text{source}}$  given by equation (5). On the other hand, for the events with  $D \gtrsim 15$  Mpc the particles come from distant sources associated with different filaments. Some of these may fly through voids and arrive with small  $\theta$ , while most are deflected significantly by the IGMFs. On the other hand, on average the time delay tends to increase with distance  $D$ , as expected.

Super-GZK protons, with  $E_{\text{obs}} > 60$  EeV come mostly from within  $D \sim 100$  Mpc. Most of them from  $D \gtrsim 15$  Mpc arrive with  $\theta \lesssim 10^\circ$  and  $t_d \lesssim 10^7$  yr (Fig. 5, *bottom*). Since the volume filling factor for  $B$  greater than a few times  $10^{-8}\text{G}$  (corresponding to  $r_g \sim 2 - 3$  Mpc) is small, those particles could travel almost rectilinearly through void regions, avoiding the strongly magnetized regions of clusters and groups.

In Figure 6, the distribution of recorded events is shown in the  $(E_{\text{obs}}, \theta)$  and  $(E_{\text{obs}}, \log t_d)$  planes. The events recorded in all six  $\Lambda$ CDM simulations are included and  $\gamma = 2.7$  and  $D_{\text{min}} = 3$  Mpc are used. On average the deflection angle decreases with energy, but a clear transition from the diffusive transport regime to the rectilinear propagation regime is apparent around  $E_{\text{obs}} \sim E_{\text{GZK}}$ . Sub-GZK particles, with long interaction lengths and small gyroradii, are strongly scattered, while super-GZK particles, with short interaction lengths and large gyroradii, are much less affected. As expected, the time delay decreases with increasing energy on average but has a rather wide spread at any given energy. For comparison, the rectilinear flight time for the mean separation of sources,  $l_s = 40$  Mpc, is  $t_{\text{rec}} \equiv l_s/c \approx 10^8$  yr.

Figure 7 shows the fractions of recorded events in all six  $\Lambda$ CDM simulations as functions of  $\theta$  and  $t_d$ ,  $df/d\theta$  and  $df/d\log t_d$ , and their cumulative distributions. The events are divided into three energy channels as in Figure 5, and each curve is normalized by the total number of events in the corresponding channel. In order to demonstrate the dispersion of the statistics due to cosmic variance, we also plot the error bars in the cumulative distributions, which are calculated as the standard deviations of the values of  $f$  for the six simulations.

In the lowest energy channel ( $10 \text{ EeV} < E_{\text{obs}} < 30 \text{ EeV}$ , *red lines*), the deflection angle is quite large, with about 70% of the events arriving with  $\theta > 30^\circ$ , that is,  $f(> 30^\circ) \approx 0.7$ . Moreover, with  $f(> 10^8 \text{ yr}) \approx 0.7$  the time delay is much longer than the typical lifetimes of AGNs ( $\tau_{\text{AGN}} = 0.01 - 0.1$  Gyr). In the highest energy channel ( $E_{\text{obs}} \geq 60 \text{ EeV}$ , *black lines*), on the other hand, about 70 % of the recorded events arrive with a deflection angle smaller than  $\sim 15^\circ$  and a time delay less than  $\sim 10^7$  yr. About 35 % arrive with an angle smaller than  $\sim 5^\circ$ . This implies that the arrival direction of super-GZK cosmic rays may show a positional correlation with the source AGNs and also with the LSS, and the source AGNs are very likely to still be active for such events. We note, however, that these results are not restricted to the specific AGN model. They can be applied for any UHECR sources that have a spatial distribution and magnetic field environment similar to those of luminous X-ray clusters.

We note that the present work produces results different from what previous studies have predicted (Armengaud *et al.* 2005; Dolag *et al.* 2005). Specifically, the deflection angle is smaller than that found by Sigl *et al.* but larger than that of Dolag *et al.*. This should be attributable to the difference in the models for the IGMFs, as discussed in §2.1. We also note that the effects of Galactic magnetic fields are not included in our analysis. Recently, Takami & Sato (2007), for instance, considered several different models for the Galactic magnetic fields and predicted that the deflection angle of  $10^{19.8}$  eV protons should be greater than  $8^\circ$  toward the Galactic center, while being mostly  $3 - 5^\circ$  outside a circular region of

30° radius around the Galactic center.

### 3.2. Predicted Energy Spectrum

Here we present the energy flux,  $J(E_{\text{obs}})$ , of the recorded cosmic-ray events in our propagation experiment. By applying a weighting factor proportional to  $E_{\text{inj}}^{-\gamma}$  to each recorded particle, the energy spectra for different values of  $\gamma$  can be constructed. The predicted spectra are calculated for injection spectra with  $\gamma$ -values of 2.0, 2.4, and 2.7 and for  $D_{\text{min}} = 3$  and  $D_{\text{min}} = 10$  Mpc. Again, all data from the six  $\Lambda$ CDM simulations are combined. Figure 8 shows the resulting spectra,  $J(E)$ , along with the data observed at AGASA (Nagano & Watson 2000), HiRes-I (Berezinsky *et al.* 2006), HiRes-II (Zech 2004), and Auger (Parizot *et al.* 2007). Since the amplitude of the injection spectrum is not specified, the amplitude of the predicted  $J(E)$  is arbitrary in our model. Therefore each curve was adjusted by eye to fit the HiRes data below  $E_{\text{GZK}}$ .

The presence of GZK suppression above 60 EeV is obvious in all the predicted spectra and the observed data except for the AGASA data. The predicted spectra for  $\gamma = 2.4 - 2.7$  are all consistent with the observed data, again with the exception of the AGASA data.

As shown in the bottom panel of Figure 8, our work predicts that above  $\sim 100$  EeV the flux is much higher with  $D_{\text{min}} = 3$  Mpc than with  $D_{\text{min}} = 10$  Mpc, indicating that the contribution from nearby sources is important. Thus, if the injection spectrum has a power-law distribution extending well beyond the GZK energy as we assume here, the implication is that the Auger experiment, which has Centaurus A in its field of view, may see a higher flux of super-GZK cosmic rays, compared with experiments in the Northern Hemisphere such as HiRes and the Telescope Array (Fukushima *et al.* 2007). However, it is quite possible that the injection spectrum is limited to a maximum energy  $E_{\text{max}}$  set by the age and size of the astrophysical accelerators or by the GZK energy loss at the acceleration sites. Moreover, the value of  $E_{\text{max}}$  may vary with the properties of the accelerator, rather than maintaining a constant value of  $10^3$  EeV. In order to settle this issue, much better statistics for the energy spectrum and the arrival directions above 100 EeV are needed.

## 4. Summary and Discussion

In the search for the astrophysical sources of UHECRs, it is important to understand how the propagation of these charged particles is affected by intergalactic magnetic fields in the large-scale structure of the universe. On the other hand, the information imprinted

on the distribution of the UHECR arrival directions may help us to understand the nature of the IGMFs and their roles in the formation and evolution of the LSS and constituent galaxies. Considering the limitations of current observational techniques in measuring the IGMFs in very low density regions such as filaments and voids, it is crucial to construct a physically motivated model to estimate the IGMFs in the LSS.

In this study, we adopted a new model based on the turbulence dynamo (Ryu *et al.* 2008) to predict the strength of the IGMFs. The magnetic field energy is estimated from the local vorticity and turbulent kinetic energy of flow motions in cosmological simulations of the LSS formation in a concordance  $\Lambda$ CDM universe. For the direction of the IGMFs, the topology of the passive magnetic fields followed in the cosmological simulations is used. This approach provides an IGMF model that is independent of the initial seed fields and does not require any renormalization to yield the observed field strength in the intracluster medium. We predict highly structured IGMFs with characteristic field strengths on the order of  $10^{-6}$  G in clusters of galaxies and  $10^{-8}$  G in filaments. The fields should be much weaker in sheets and voids.

Protons with  $10 \text{ EeV} \leq E_{\text{inj}} \leq 10^3 \text{ EeV}$  are injected at the locations of luminous X-ray clusters with  $kT > 1 \text{ keV}$ . These sources may represent a population of AGNs residing inside host clusters. This X-ray temperature criterion naturally places the sources at strongly magnetized regions with  $B_s \sim 0.1 \mu\text{G}$  with a comoving density of  $2 - 3 \times 10^{-5} (h^{-1} \text{Mpc})^{-3}$ . Then the propagation of the UHE protons is followed through the structured IGMFs, including the energy losses due to interactions with the cosmic background radiation. The UHE protons are recorded at the positions of mock observers located in groups of galaxies, with halo temperatures in the range  $0.05 \text{ keV} < kT < 0.5 \text{ keV}$ .

Below the GZK energy, the UHE protons come from sources as distant as  $\sim 1 \text{ Gpc}$ . They are significantly scattered by the IGMFs, resulting in a wide range of deflection angles, up to  $180^\circ$ , and have time delays ranging from  $10^7$  to  $10^{9.5} \text{ yr}$ . On the other hand, the protons above 60 EeV come mostly from sources within  $\sim 100 \text{ Mpc}$ . About 70% of them avoid strong deflection and arrive at the observers within  $\sim 15^\circ$  of their source position on the sky with a time delay of less than  $\sim 10^7 \text{ yr}$ . About 35% arrive within  $\sim 5^\circ$ . This implies that there may exist a correlation between the arrival direction of super-GZK cosmic rays and the sky position of the corresponding AGNs. We thus conclude that in the present scenario, UHECR astronomy may be possible at  $E > 60 \text{ EeV}$ . Our prediction seems to be consistent with a recent report by the Auger Collaboration (Abraham *et al.* 2007) in which the arrival directions of cosmic rays above 60 EeV in their data were found to be correlated with the sky position of AGNs within 75 Mpc.

For any cosmological sources, we expect to see GZK suppression in the energy spectrum

of UHECRs if the injection spectrum has a power-law distribution and extends well beyond the GZK energy. In this case, nearby sources, within 10 – 20 Mpc, are expected to make a significant contribution to the flux above  $\sim 100$  EeV.

Finally, as recently reported by Auger (Unger *et al.* 2007), some UHECRs might be heavy nuclei. In the cosmological-shock model, for example, protons can be accelerated up to a few times 10 EeV, so heavy nuclei should dominate the particle flux above that energy (Kang *et al.* 1997; Inoue *et al.* 2007). In a future study, we will consider the propagation of heavy nuclei from cosmological sources in our model IGMFs, taking into account photo disintegration, photo pair production, and photo pion production processes. We expect that the propagation of UHE iron nuclei ( $Z = 26$ ), at least, will be in the diffusive transport regime as a results of their much smaller gyroradius ( $r_g \propto E/Z$ ) (Armengaud *et al.* 2005). For intermediate-mass nuclei such as He, C, N, and O, detailed propagation simulations including secondary particles produced by photo disintegrations are necessary in order to determine whether astronomy with UHE nuclei is possible or not.

The work of H. K. and S. D. is supported by Korea Science and Engineering Foundation through the Astrophysical Research Center for the Structure and Evolution of the Cosmos (ARCSEC). The work of D. R. and J. C. is supported by Korea Research Foundation grants funded by the Korean Government (MOEHRD) (KRF-2007-341-C00020 and KRF-2006-331-C00136, respectively). This work was also supported by the Korea Foundation for International Cooperation of Science and Technology through the grant K20702020016-07E0200-01610.

## REFERENCES

- Abbasi, R. U. *et al.* (High Resolution Fly’s Eye Collaboration) 2005, ApJ, 622, 910
- Abbasi, R. U. *et al.* (High Resolution Fly’s Eye Collaboration) 2006, ApJ, 636, 680
- Armengaud, E., Sigl, G., & Miniati, F. 2005, Phy. Rev. D., 72, 043009
- Armengaud, E. *et al.*, (Pierre Auger Collaboration) 2007, Proc. 30th Int. Cosmic-Ray Conf. (Merida), arXiv0706.2640
- Berezinsky, V. S., & Grigor’eva, S. I. 1988, A&A, 199, 1
- Berezinsky, V. S., Gazizov, A., & Grigor’eva, S. I. 2006, Phys. Rev. D., 74, 043005
- Biermann, P. L. & Strittmatter, P. A. 1987, ApJ, 322, 643

- Blasi, P. & De Marco, D. 2004, *Astropart. Phys.*, 20, 559
- Burgett, W. S. & O’Malley, M. R. 2003, *Phys. Rev. D.*, 67, 092002
- Dolag, K., Grasso, D., Springel, V., & Tkachev, I. 2004, *JETP. Lett.*, 79, 583
- Dolag, K., Grasso, D., Springel, D., & Tkachev, J. 2005, *Journal of Cosmology and Astroparticle Physics*, 1, 009
- Facal, P. *et al.*, (Pierre Auger Collaboration) 2007, *Proc. 30th Int. Cosmic-Ray Conf. (Merida)*, arXiv0706.4322
- Ferrarese, L, Mould, J. R., Stetson, P. B., Tonry, J. L., Blakeslee, J. P., & Ajhar, E. S. 2007, *ApJ*, 654, 186
- Fukushima, M. *et al.* (Telescope Array collaboration) 2007, *Proc. 30th Int. Cosmic-Ray Conf. (Merida)*
- Harari, D. *et al.*, (Pierre Auger Collaboration) 2007, *Proc. 30th Int. Cosmic-Ray Conf. (Merida)*, arXiv0706.1715
- Hillas, A. M. 1984, *ARA&A*, 22, 425
- Inoue, S., Sigl, G., Miniati, F., & Armengaud, E. 2007, preprint (astro-ph/0701167)
- Greisen, K. 1966, *Phys. Rev. Lett.*, 16, 748
- Kang, H., Rachen, J. P., & Biermann, P. L. 1997, *MNRAS*, 286, 25
- Kang, H., Ryu, D., & Jones, T. 1996, *ApJ*, 456, 422
- Kang, H., Ryu, D., Cen, R., & Ostriker, J. P. 2007, *ApJ*, 669, 729
- Kulsrud, R. M., Cen, R., Ostriker, J. P., & Ryu, D. 1997, *ApJ*, 480, 481
- Mei, S., Blakeslee, J. P., Cote, P., Tonry, J. L., West, M. J., Ferrarese, L., Jordan, A., Peng, E. W., Anthony, A., & Merritt, D. 2007, *ApJ*, 655, 144
- Nagano, A. & Watson, A. A., 2000, *Rev. Mod. Phys.*, 72, 689
- Parizot, E. *et al.*, (Pierre Auger Collaboration) 2007, *proceedings for the the International Symposium on Astronomy and Astrophysics of Extreme Universe*, arXiv0709.2500
- Abraham, J. *et al.* 2007, *Science*, 318, 939

- Pravdin, M. I. et al. (Yakutsk collaboration) 1999, proceedings for the 26th ICRC (Salt Lake City, USA), 3, 292
- Rasmussen, J. & Pedersen, K. 2001, ApJ, 559, 892
- Ryu, D., Kang, H., & Biermann, P. L. 1998, A&A, 335, 19
- Ryu, D., Kang, H., Cho, J., & Das, S. 2008, Science, 320, 909
- Sigl, G., Miniati, F., & Ensslin, T. A. 2003, Phys. Rev. D., 68, 043002
- Sigl, G., Miniati, F., & Ensslin, T. A. 2004, Phys. Rev. D., 70, 043007
- Takami, H. & Sato, K. 2007, arXiv0711.2386
- Takeda, M. *et al.* 1999, ApJ, 522, 225
- Tinyakov, P. G. & Tkachev, I. I. 2001, JETP Lett., 74, 445
- Unger, M. *et al.*, (Pierre Auger Collaboration) 2007, Proc. 30th Int. Cosmic-Ray Conf. (Merida), arXiv0706.1495
- Uchihori, Y., Nagano, M., Takeda, M., Teshima, M., Lioyd-Evans, J., & Watson, A. A. 2000, Astropart. Phys., 13, 151
- Watson, A. A. 2006, Nucl. Phys. Proc. Suppl., 151, 83
- Waxman, E. Phys. Rev. Lett., 75, 386
- Yoshiguchi, H., Nagataki, S., & Sato, K. 2003, ApJ, 592, 311
- Zatsepin, G. T. & Kuzmin, V. A. 1966, JETP Lett., 4, 78
- Zech, A. *et al.* (High Resolution Fly’s Eye Collaboration) 2004, Nuclear Physics B (Proc. Suppl.), 136, 34

Table 1. Numbers of Sources and Observers

Simulation	Sources	Observers
$\Lambda$ CDM1	18	1000
$\Lambda$ CDM2	31	1344
$\Lambda$ CDM3	20	1379
$\Lambda$ CDM4	29	1336
$\Lambda$ CDM5	24	1343
$\Lambda$ CDM6	28	1365



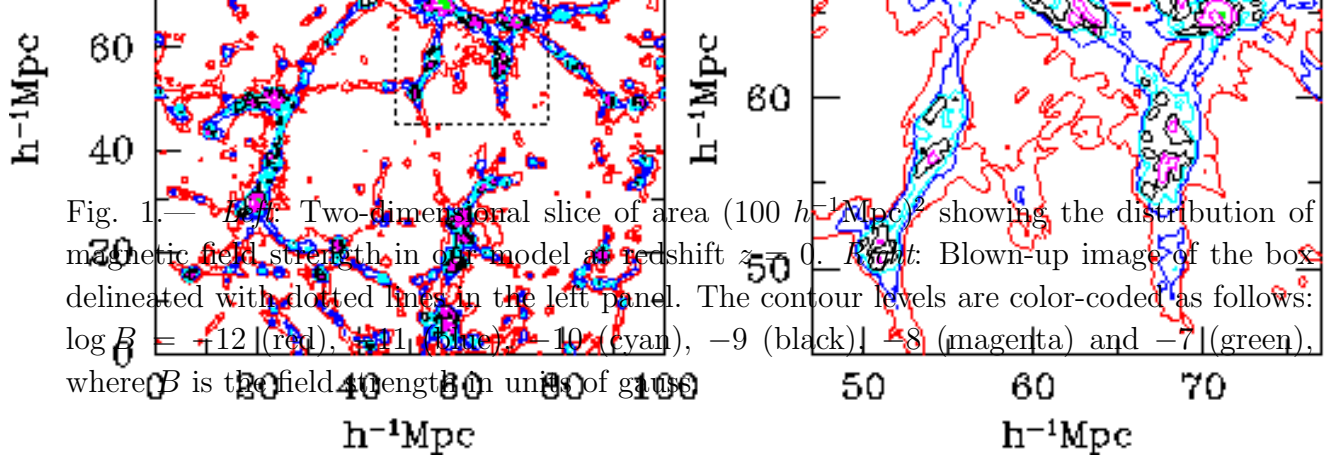


Fig. 1.— *Left*: Two-dimensional slice of area  $(100 h^{-1} \text{Mpc})^2$  showing the distribution of magnetic field strength in our model at redshift  $z=0$ . *Right*: Blown-up image of the box delineated with dotted lines in the left panel. The contour levels are color-coded as follows:  $\log B = -12$  (red),  $-11$  (blue),  $-10$  (cyan),  $-9$  (black),  $-8$  (magenta) and  $-7$  (green), where  $B$  is the field strength in units of gauss.

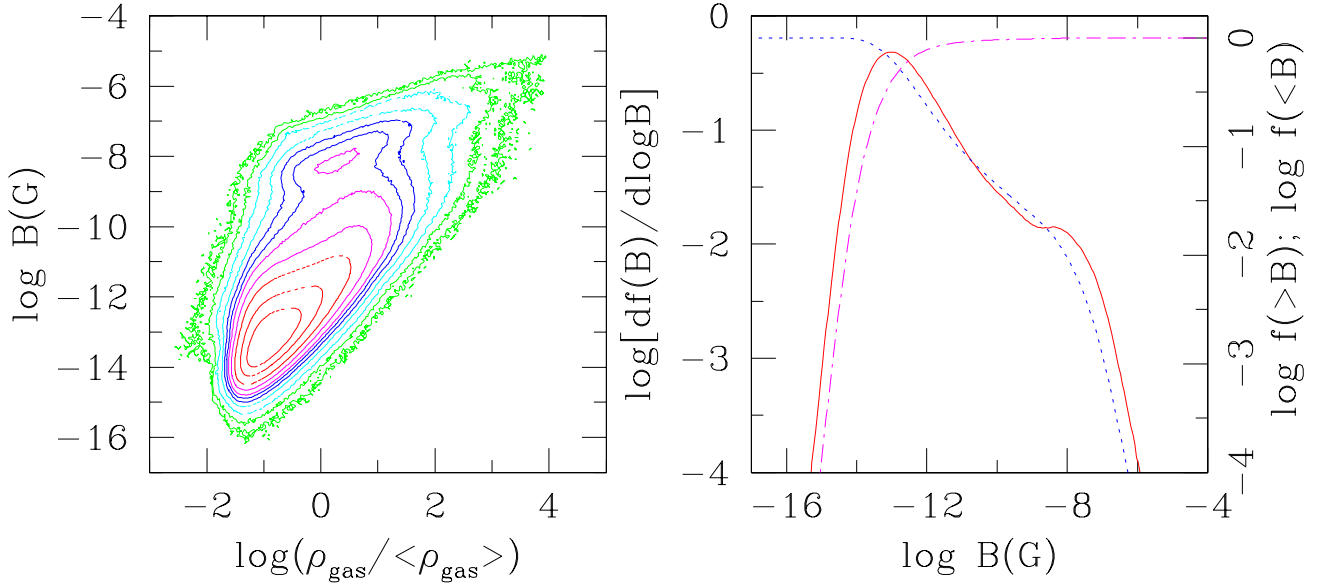


Fig. 2.— *Left*: volume fraction in the gas density vs. field strength plane with our model IGMFs at redshift  $z=0$ . *Right*: volume fraction,  $df/d\log B$  (solid line), and its cumulative distributions,  $f(> B)$  (dotted line) and  $f(< B)$  (dot-dashed line) as a function of the IGMF strength.

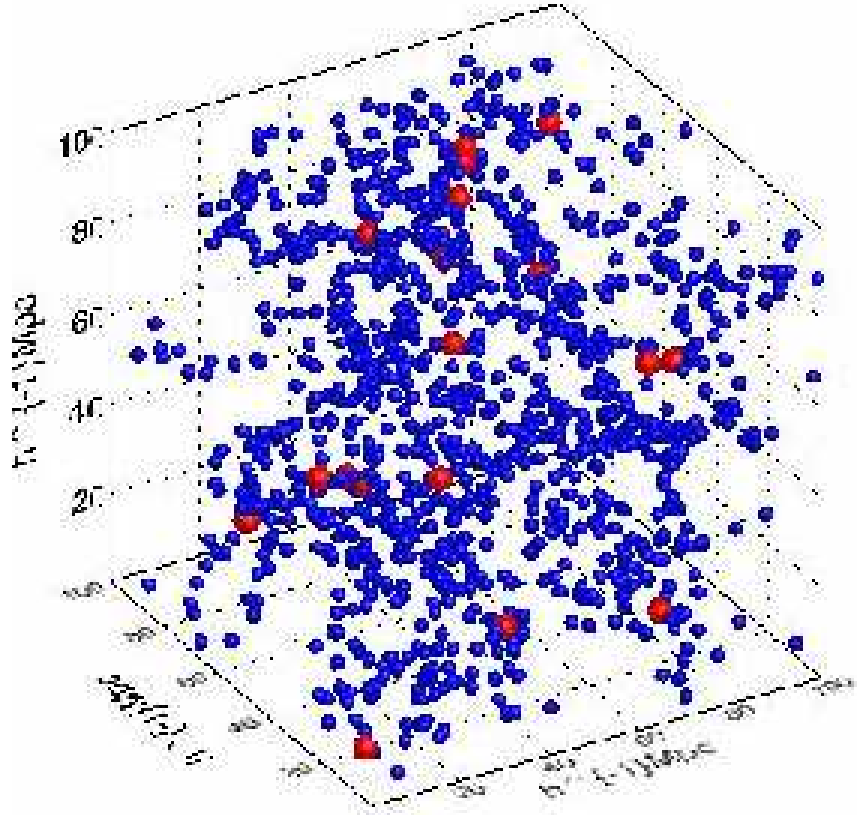


Fig. 3.— Distribution of UHECR sources (*red circles*) and mock observers (*blue circles*) in simulation  $\Lambda$ CDM1. Sources are modeled as AGNs inside X-ray clusters, while mock observers are placed inside groups of galaxies similar to the Local Group.

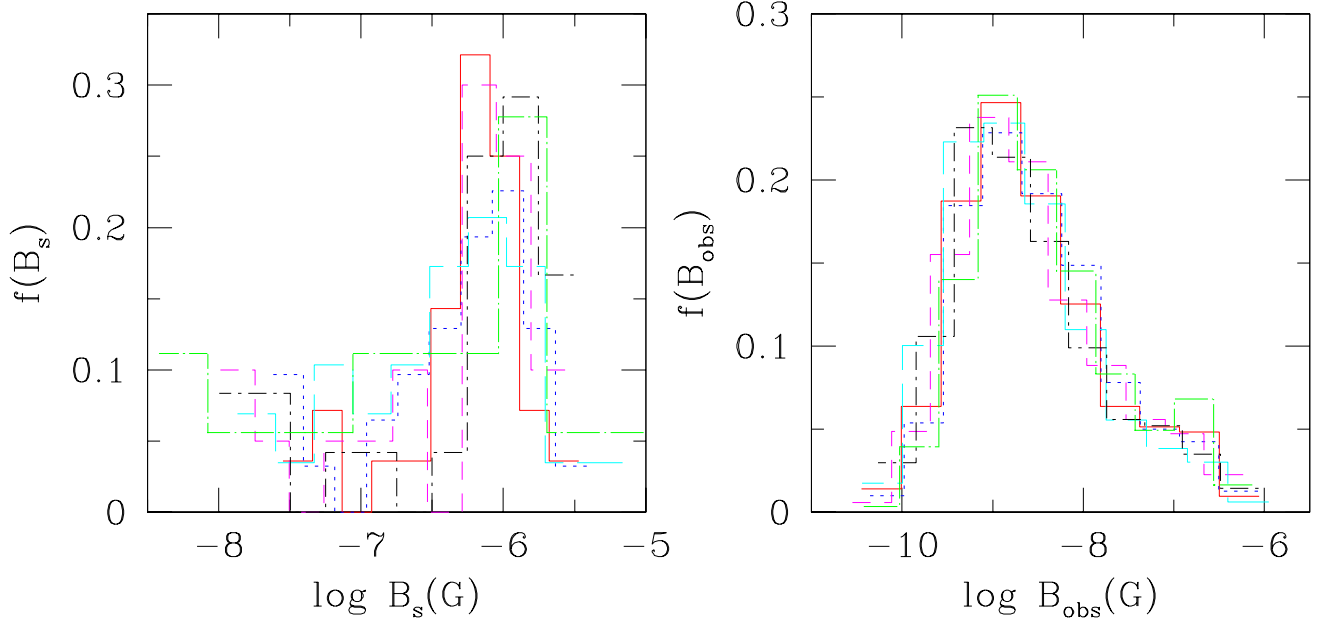


Fig. 4.— *Left*: Distribution of magnetic field strength at source locations in the six simulations with different initial conditions. Different line styles are used for simulations  $\Lambda\text{CDM1}$  -  $\Lambda\text{CDM6}$ . *Right*: Distribution of magnetic field strength within the observer spheres. The same line styles as in the left panel are used.

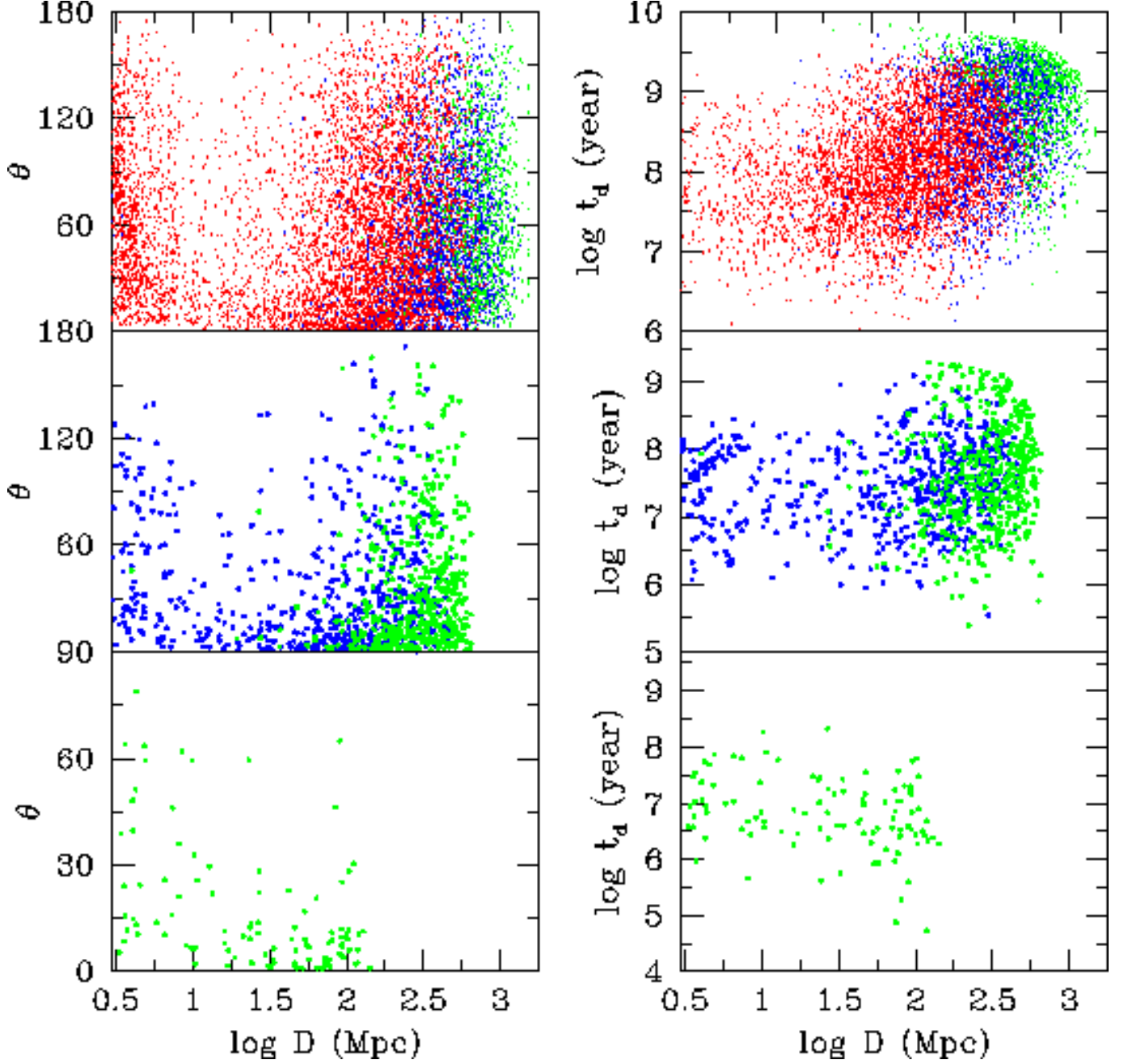


Fig. 5.— Deflection angle ( $\theta$ ) and time delay ( $t_d$ ) as functions of the source-to-observer distance ( $D$ ). The events recorded with observed energies  $10 \text{ EeV} \leq E_{\text{obs}} < 30 \text{ EeV}$  are shown in the top panels,  $30 \text{ EeV} \leq E_{\text{obs}} < 60 \text{ EeV}$  in the middle panels, and  $E_{\text{obs}} \geq 60 \text{ EeV}$  in the bottom panels. The data points are color-coded by the injection energy as follows: red,  $10 \text{ EeV} \leq E_{\text{inj}} < 30 \text{ EeV}$ ; blue,  $30 \text{ EeV} \leq E_{\text{inj}} < 60 \text{ EeV}$ ; green,  $E_{\text{inj}} \geq 60 \text{ EeV}$ . An injection spectrum  $N(E_{\text{inj}}) \propto E_{\text{inj}}^{-2.7}$  is assumed. (See text for details.)

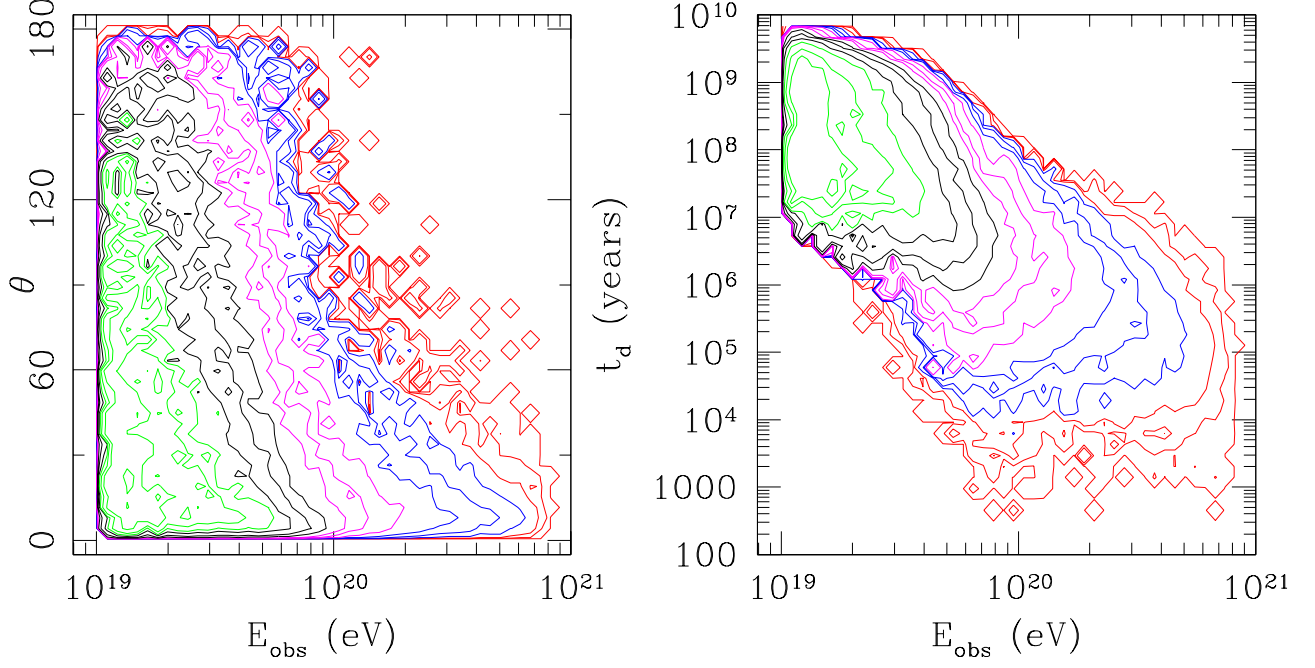


Fig. 6.— Distribution of observed UHECR events in the planes of observed energy vs. deflection angle (*left*) and time delay (*right*). The events recorded in all six  $\Lambda$ CDM simulations are included, and  $\gamma = 2.7$  and  $D_{\min} = 3$  Mpc were used.

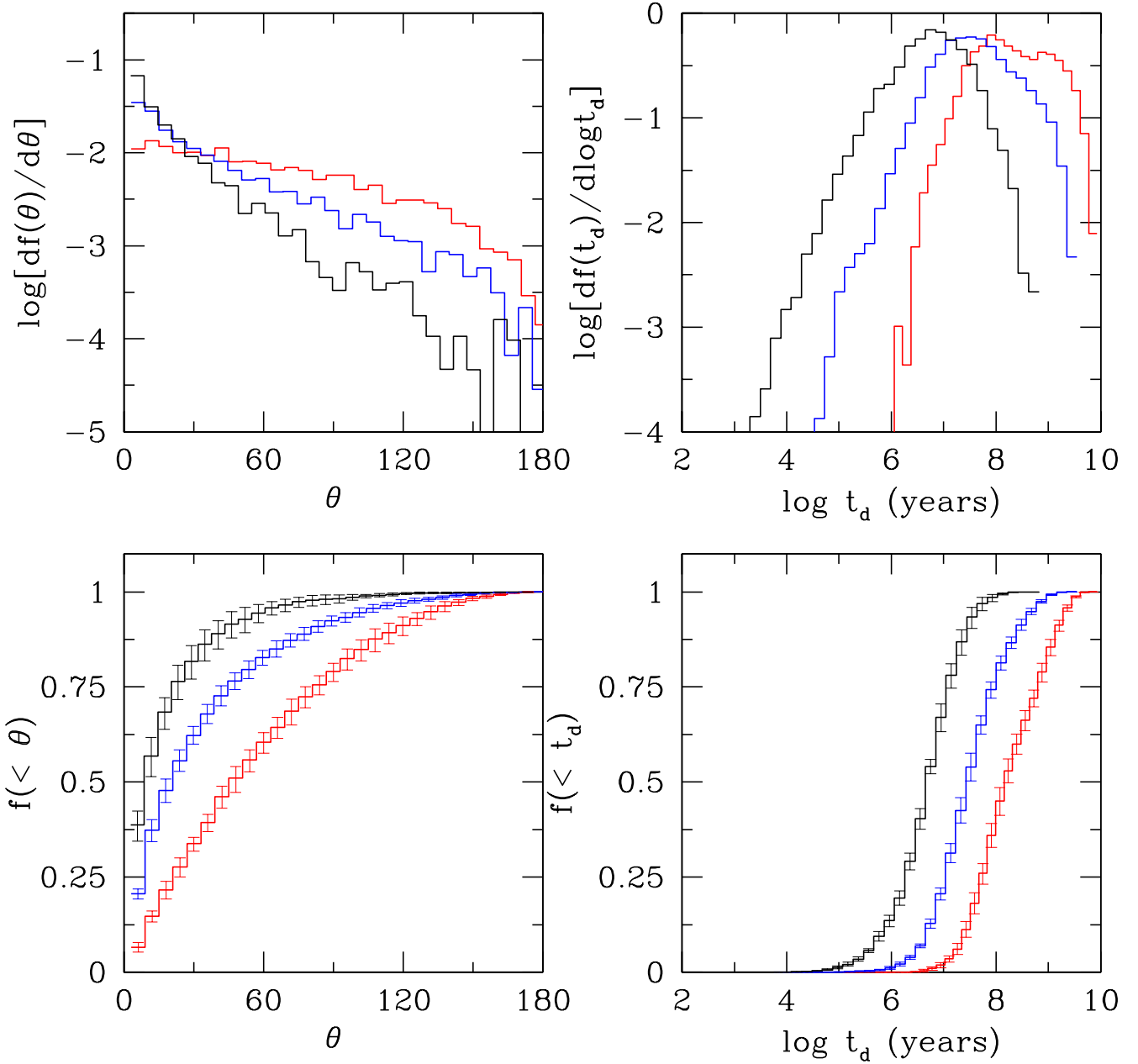


Fig. 7.— Fractions of observed UHECR events as a function of deflection angle (*top left*) and time delay (*top right*), and the respective cumulative distributions (*bottom*). The events recorded in all six  $\Lambda$ CDM simulations are included, and  $\gamma = 2.7$  and  $D_{\min} = 3$  Mpc were used. The distributions for different energy channels are shown: red,  $10 \text{ EeV} < E_{\text{obs}} < 30 \text{ EeV}$ ; blue,  $30 \text{ EeV} \leq E_{\text{obs}} < 60 \text{ EeV}$ ; black,  $E_{\text{obs}} \geq 60 \text{ EeV}$ . The error bars shown for the cumulative distributions are the standard deviations of  $f$  for the six simulations.

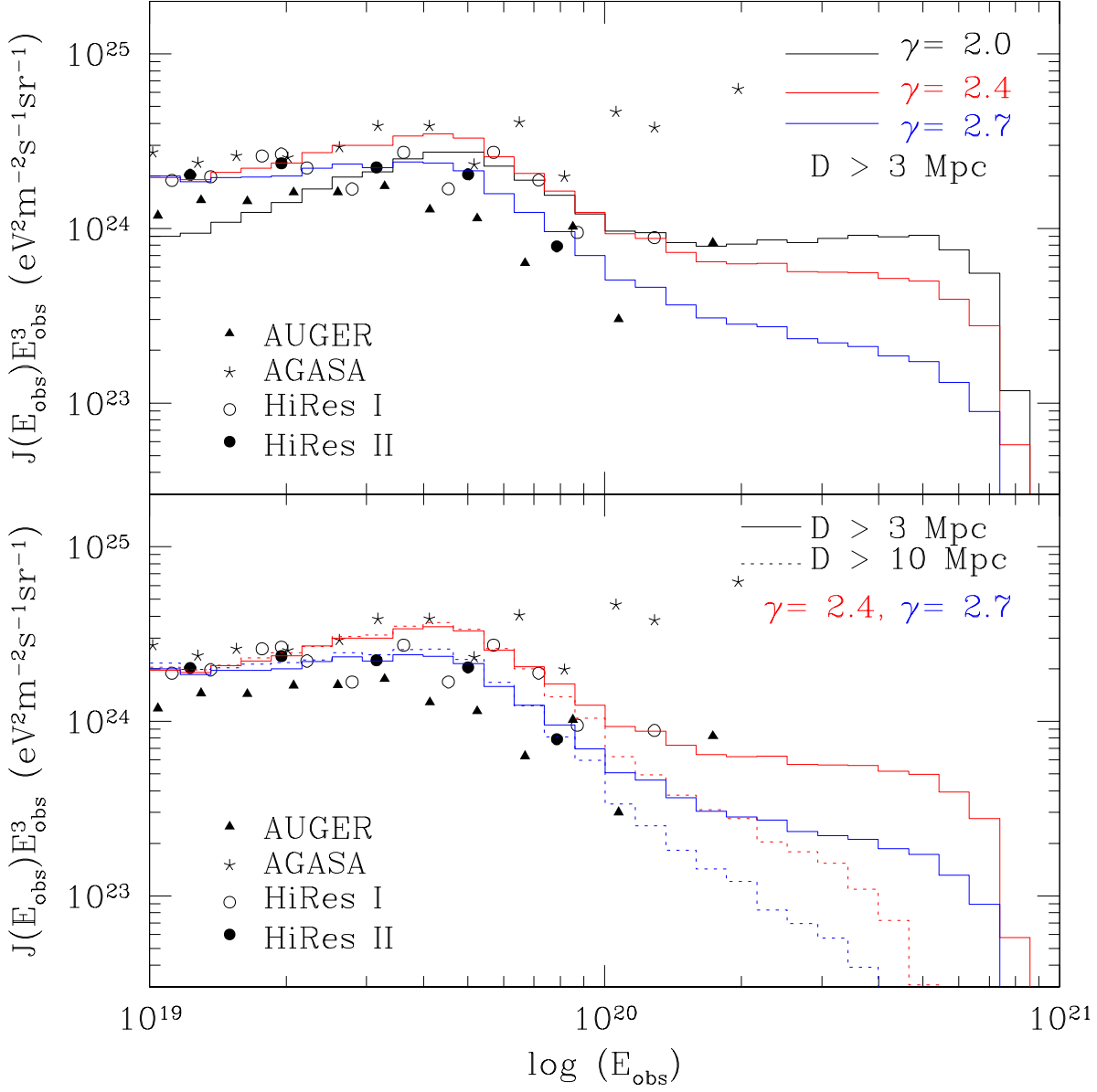


Fig. 8.— Energy spectra of UHE protons predicted by our model. The injection spectrum at the sources is proportional to  $E_{\text{inj}}^{-\gamma}$  for  $10 \leq E_{\text{inj}} \leq 10^3$  EeV. *Top*: The blue, red, and black lines are for  $\gamma$ -values of 2.0, 2.4, and 2.7, respectively, with a minimum source-to-observer distance  $D_{\text{min}} = 3$  Mpc. *Bottom*: The red lines are for an injection spectrum with  $\gamma = 2.4$ , while the blue lines are for  $\gamma = 2.7$ . The solid lines are for  $D_{\text{min}} = 3$  Mpc, and the dotted lines are for  $D_{\text{min}} = 10$  Mpc. The data observed at AGASA (Nagano & Watson 2000), HiRes-I (Berezinsky *et al.* 2006), HiRes-II (Zech 2004), and Auger (Parizot *et al.* 2007) are marked with asterisks, open circles, filled circles, and triangles, respectively. The predicted spectra were arbitrarily scaled by eye to fit the HiRes data below  $E_{\text{GZK}}$ .